Azimuthal Induced Current Formation and Ion Acceleration in an Inductive Radiofrequency Plasma Thruster

IEPC-2019-A-775

Presented at the 36th International Electric Propulsion Conference
University of Vienna • Vienna, Austria
September 15-20, 2019

H. Sekine[1], H. Koizumi[2], and K. Komurasaki[3]
The University of Tokyo, Kashiwa, Chiba, 277-0871, Japan

Abstract: Applied and plasma-induced magnetic field distribution are measured in an electrodeless plasma thruster using a three-directional B-dot probe. Time- and space- resolved distributions of the azimuthal induced current are obtained using a Gaussian fitting analysis. Its distributions are in a good agreement with those of the azimuthal electric field, ensuring the inductive current drive. The ion dynamics are also investigated by the time-of-flight technique using the ion saturation current of a Langmuir probe. Without the external dc magnetic field, the ion flow velocity is estimated as comparable to the ion sound speed. In the external dc magnetic field, generation of supersonic ion flow is indicated.

Nomenclature

μ_0	=	vacuum permeability
k_B	=	Boltzmann constant
j_θ	=	azimuthal plasma current
PM	=	permanent magnet
BP	=	B-dot probe
LP	=	Langmuir probe
$\boldsymbol{B}_{\mathrm{ext}}$	=	applied ac magnetic field
$\boldsymbol{B}_{\mathrm{w/p}}$	=	total ac magnetic field in the plasma
$\Delta\boldsymbol{B}$	=	plasma-induced magnetic field
I_{acc}	=	current in the acceleration coil
ω	=	frequency of the current in the acceleration coil
E_θ	=	azimuthal electric field
I_{is}	=	ion saturation current
T_{e}	=	electron temperature
m_i	=	xenon ion mass
V	=	estimated plasma flow velocity
C_{S}	=	ion sound speed
E_{V}	=	flow energy of the plasma
E_{T}	=	thermal energy of the plasma

[1] Ph. D student, Department of Advanced Energy, sekine@g.ecc.u-tokyo.ac.jp
[2] Associate Professor, Department of Advanced Energy, koizumi@al.t.u-tokyo.ac.jp
[3] Professor, Department Aeronautics and Astronautics, komurasaki@al.t.u-tokyo.ac.jp

I.Introduction

Developing electrodeless plasma thrusters (EPTs) are attractive topics for future deep space explorations, cargo missions, and piloted missions.[1] Since the EPTs ionize the propellant gas and expel it with no electrodes directly touching to the plasma, they can avoid erosion of the electrodes, which is one of the most challenging matters for the conventional plasma thrusters, e.g. Hal effect thrusters[2] and ion thrusters.[3] It leads a longer lifetime of the propulsion system.

Basic EPTs have a cylindrical source tube made of dielectric material and accelerate plasmas along the axial direction toward the open source exit. A variety of combinations of the plasma production and acceleration mechanisms have been proposed. A variable specific impulse plasma rocket (VASIMR)[4] utilizes radiofrequency (rf)/helicon plasmas, and ion cyclotron resonance heating (ICRH)[5] with magnetic nozzle for acceleration. Helicon thrusters accelerate high-density rf/helicon plasmas by a magnetic nozzle[6], or other acceleration methods[7]. Recently, physics in the magnetic nozzle and resultant plasma acceleration have been discussed numerically[8] and experimentally[9]. Understanding the interaction between a magnetic nozzle and the plasma leads to the improvement of performance of the thrusters up to *O*(~10 mN/kW).

Some of the electrodeless thrusters utilize electromagnetic acceleration. The features of this type of acceleration are inductive production of the azimuthal current loop/sheet j_θ via an external coil and the plasma acceleration by axial Lorentz force $f_z = j_\theta B_r$. Pulsed inductive thrusters (PITs)[10] employ Townsend-like discharges and accelerate them electromagnetically. Faraday Acceleration with Radio-frequency Assisted Discharge (FARAD)[11] introduces rf discharge as pre-ionization to lower the necessary high voltage for PITs to ionize propellant gas. In order to suppress the plasma loss to the wall of the FARAD, Radio-frequency Inductive Accelerator with Low-aspect-ratio Plasma (RIPAL) conducts rf plasma production and acceleration in the same region[12]. In addition to that, it accelerates plasma utilizing low-frequency (*O*(10-100 kHz)) diverging magnetic field instead of pulsed diverging magnetic field aiming the improvement of propellant utilization efficiency. Thrust measurements with a target-type thrust stand showed the thrust-to-power ratio of the RIPAL of ~2 mN/kW. To improve the performance of those inductive EPTs, the detailed insight of the electromagnetic acceleration process and resultant momentum transportation is essential. In this study, the spatiotemporal distributions of azimuthal induced electric current j_θ and radial magnetic field B_r were resolved by B-dot probe measurements. The distributions of the azimuthal currents correspond to the azimuthal electric field, indicating the current formation is mainly derived by the electric field. With the induced current measurements, the plasma acceleration process was investigated by the measurements of the spatiotemporal distributions of ion saturation currents of a Langmuir probe. It was found that the relationship between the azimuthal current formation and resultant plasma acceleration. Moreover, it is shown that the static (dc) magnetic field has a important role in the ion acceleration.

II.Experimental Setup

A. Vacuum facility and Thruster setup

A schematic of the experimental setup is shown in Figure 1(a). The RIPAL is composed of a glass cylinder, a triple-turn rf antenna, a PTFE backplate, permanent magnets, and an acceleration coil. The glass cylinder is contiguously connected to a vacuum chamber of diameter of ~1.4 m and length ~3 m, which is evacuated by a cryopump to a pressure of ~8×10^{-4} Pa when the thruster is not operated and ~2×10^{-2} Pa during the thruster is in operation. Xenon gas is introduced as the propellant with a constant rate of 1.8 mg/s through small holes on the backplate through a mass flow controller. An rf power of 400 W is continuously input to the rf antenna through an impedance matching box, producing an rf plasma in the glass cylinder. The typical electron temperature is ~8 eV, and the electron density is ~10^{11} cm^{-3}. Permanent magnets are surrounding the glass cylinder for efficient plasma production (Figure 1(b)). The acceleration coil is located on the backplate outside of the chamber and connected to an acceleration circuit. The circuit is a general pulse-forming circuit, which is composed of four 100 nF capacitors, an IGBT switch, and a dc power supply. The capacitors are charged to 1 kV using the dc power supply, and supply an ac current to the acceleration coil with the trigger signal to the IGBT switch (Figure 1(c)). The shape of the acceleration coil is 10-turns spiral type, which has been reported that it forms a uniform induced current sheet in the PITs, which leads to high efficiency. The current in the acceleration coil is monitored by a Rogowski coil with an error of less than 1 %.

B. Magnetic and Langmuir probes

To measure the ac magnetic field in the plasma $\boldsymbol{B}_{\text{ext}}$ and plasma-induced magnetic field $\Delta\boldsymbol{B}$, a three-directional Langmuir probe is fabricated (Figure 1 (d)). The details of the probe are previously presented. The plasma-induced current $\Delta\boldsymbol{B}$ is calculated as

$$\Delta\boldsymbol{B} = \boldsymbol{B}_{\text{w/p}} - \boldsymbol{B}_{\text{ext}}, \tag{1}$$

where $\boldsymbol{B}_{\text{w/p}}$ and $\boldsymbol{B}_{\text{ext}}$ are the magnetic field in the plasma and the applied magnetic field. The azimuthal induced current j_θ in the plasma is calculated using Maxwell's law as

$$j_\theta = \frac{1}{\mu_0}\left[\frac{\partial}{\partial z}(\Delta B_r) - \frac{\partial}{\partial r}(\Delta B_z)\right]. \tag{2}$$

In order to derive the special derivation of ΔB_r and ΔB_z, a Gaussian-fitting analysis is adopted.[13] In this experiment, the axial profile of ΔB_r and the radial profile of ΔB_z are fitted by the superimposition of one- or two- Gaussians to give the best fits. Typical example of the measured radial profile of ΔB_z is shown in Figure 2.

With the induced current formation, the ion dynamics is also essential to understand the acceleration process and the momentum transfer, which leads to the thrust in the inductive EPT. We also performed the measurements of the ion saturation current I_{is} of a cylindrical rf-compensated Langmuir probe (LP). It should be noted that the bottom of the cylindrical electrode is facing the upstream the thruster so as to minimize the effect of axial plasma flow to the ion saturation current. The vias voltage to the LP is fixed to ~ -66 V. As reported previously, the electron temperature is not changed drastically in inductive EPTs; thus, I_{is} can be regarded as an indicator of the ion density.

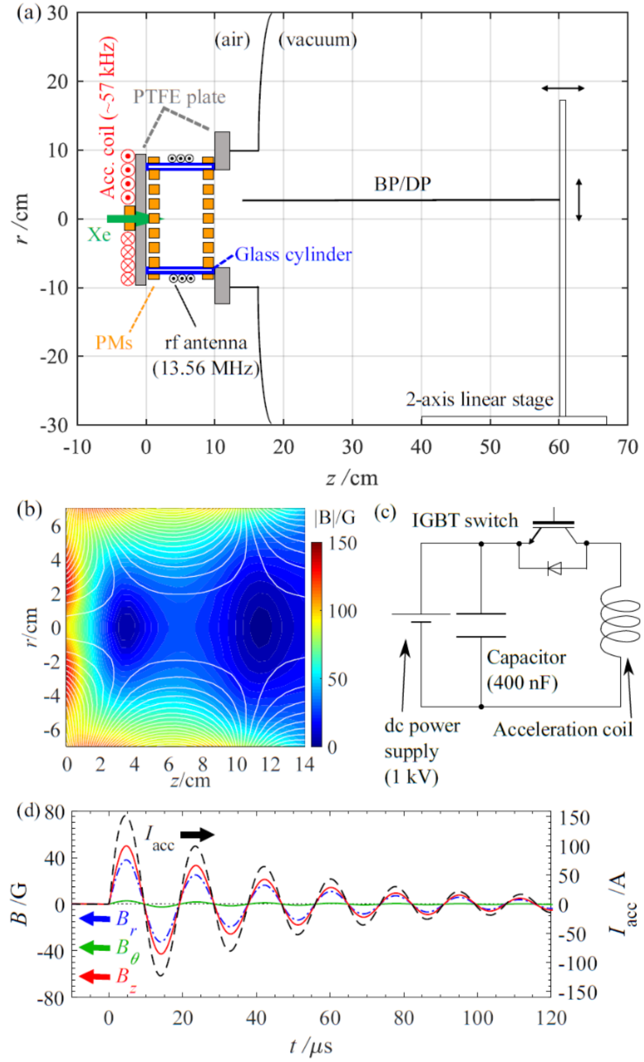

Figure 1. (a) Schematic of experimental setup. (b) External dc magnetic field applied by permanent magnets. (c) Schematic of the acceleration circuit. (d) Typical temporal evolution of the current in the acceleration coil $\boldsymbol{I}_{\text{acc}}$ and the measured magnetic field B_r, B_z, B_θ.[14]

III. Results

The spatiotemporal evolution of the plasma-induced magnetic field $\Delta\boldsymbol{B}$ and the azimuthal induced current j_θ are shown in Figure 3. The results clearly show the formation of the induced current and that of resulting plasma-induced magnetic field corresponding to the time-variation of the applied magnetic field $\boldsymbol{B}_{\text{ext}}$. The azimuthal electric field E_θ is derived from the measured magnetic field in the plasma $\boldsymbol{B}_{\text{w/p}}$, and its spatiotemporal evolution is also shown in Figure 3, showing the azimuthal induced current j_θ and the azimuthal electric field E_θ is corresponding. It ensures the current drive in the thruster is "inductive."

The spatiotemporal evolution of the ion saturation current with the dc magnetic field and without the dc magnetic field by the permanent magnets is shown in Figure 4. In both cases, the ion saturation current is increased when the ac magnetic field is applied, indicating the additional ionization with the current drive. Figure 6 shows the temporal evolution of the ion saturation current at several points along the axis. When the external dc magnetic field is not applied, the I_{is} is oscillating at twice frequency of the acceleration coil current ω, which corresponds to the applied ac magnetic field. Moreover, the I_{is} also have a peak

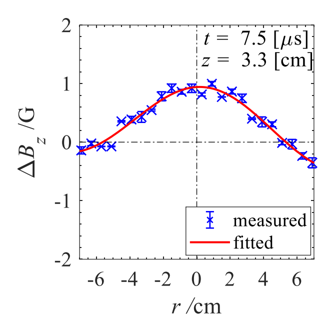

Figure 2. Typical example of the measured plasma-induced magnetic field and the fitted curve. The errorbar shows the standard error.

of the low frequency oscillation. On the other hand, with the bottom PMs, the major frequency component of the oscillation of I_{is} is ω. In this case, the low-frequency oscillation is not apparently observed. The low-frequency peak in the no-dc-magnetic-field regime and ω-frequency oscillation in the with-dc-magnetic-field regime of the I_{is} seems to be propagating downstream of the thruster with time. Figure 5 shows the temporal evolutions of the axial profile of I_{is} on axis with PMs. The propagation speed is estimated by the time-of-flight teqnique, in which linear fitting of the peaks of I_{is} give the flow velocity. The propagation speed of the low-frequency wave is ~2.7 km/s and that of the ω-frequency wave is ~4.5 km/s, respectively.

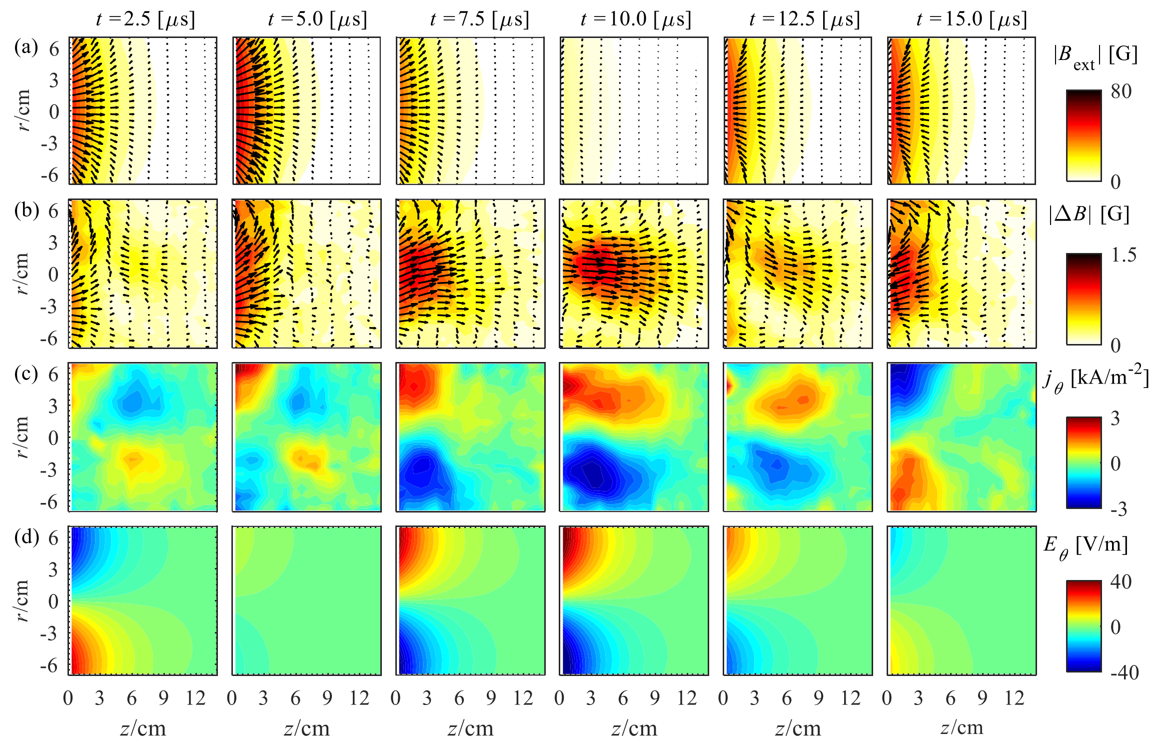

Figure 3. Measured spatiotemporal distributions of (a) ac magnetic field applied to the plasma, (b) plasma-induced magnetic field, (c) azimuthal induced current, (d) azimuthal electric field.[14]

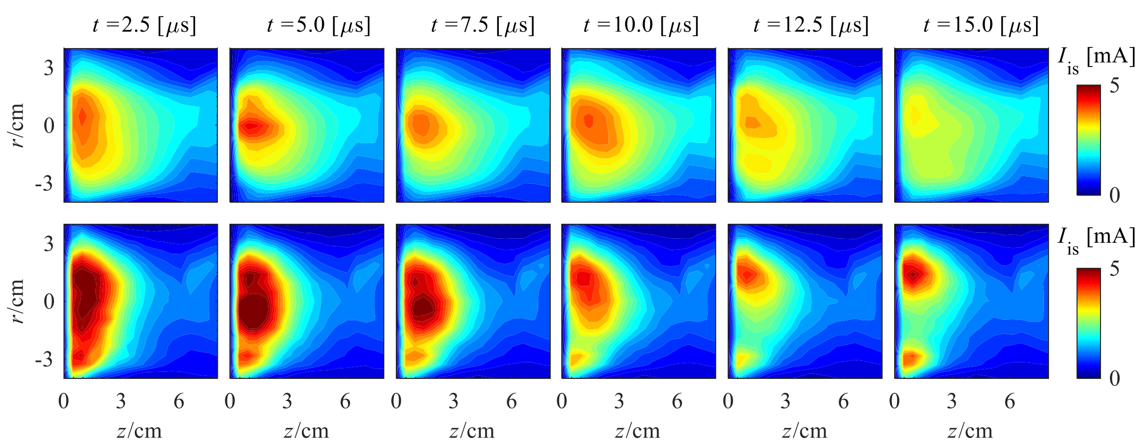

Figure 4. Measured spatiotemporal distributions of the ion saturation current of a Langmuir probe (top) with no external dc magnetic field, and (bottom) with external dc magnetic field by permanent magnets.

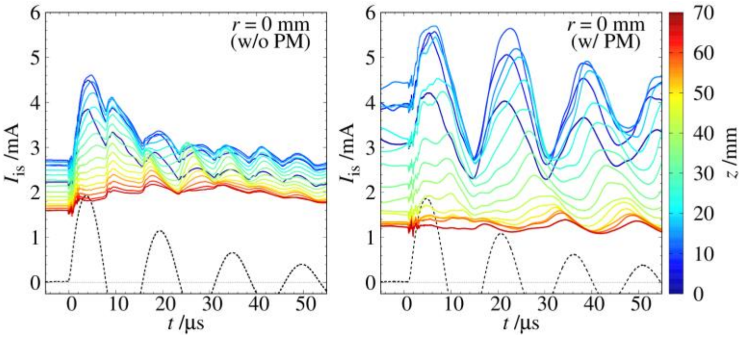

Figure 6. Temporal evolutions of the ion saturation current (left) with no external dc magnetic field, and (right) with external dc magnetic field by permanent magnets.

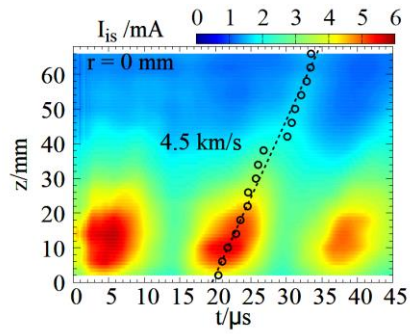

Figure 5. Temporal evolutions of the axial profile of $\boldsymbol{I_{is}}$ on the axis with PMs.

IV. Discussions

Here we regard the I_{is} propagation speed as the speed of the bulk plasma flow speed V under the assumption of quasi-neutrality and discuss the ion Mach number M_i to characterize the propagation. When the cold ion approximation is applied, the ion Mach number M_i can be defined as

$$M_i \equiv \frac{V}{C_s} \cong \frac{V}{\sqrt{k_B T_e / m_i}} = \sqrt{\frac{\frac{1}{2} m_i V^2}{\frac{1}{2} k_B T_e}} = \sqrt{\frac{E_V}{E_T}}, \tag{3}$$

where E_V is the energy of the flow, and E_T is the one-dimensional thermal energy of the plasma. Thus, the ion Mach number can be interpreted as an indicator of the ratio of the flow energy and thermal energy of the plasma. In the following estimation, $T_e \sim 10$ eV is used as a typical electron temperature.

When the dc-magnetic field is not applied, the ion Mach number M_i of the low-frequency wave is estimated as M_i~0.9, which indicates the propagation speed of the low-frequency wave is almost comparable to that of the ion sound wave. In terms of the high-frequency oscillation whose frequency is 2ω, it can be considered as the plasma production by the energy deposition to electrons via induced current, $j_\theta E_\theta$. Since the induced current j_θ and E_θ can be written as $j_\theta(t) \cong j_0 \sin(\omega t)$ and $E_\theta(t) \cong E_0 \sin(\omega t)$, the energy deposited to electrons can be expressed as $j_\theta E_\theta \cong j_0 E_0 \sin^2(\omega t)$, as seen in Fig xxx. It indicates, in this regime, the electrons are heated by the induced current leading to additional ionization, and then the density oscillation propagates as an ion sound wave. In this situation, the plasma flow energy E_V does not exceed the plasma thermal energy E_T.

As the dc-magnetic field is applied, the ion Mach number M_i of the ω-frequency is estimated as M_i~1.5. It indicates the plasma is accelerated with the current drive to higher speed than the ion sound speed; supersonic. In this situation, the plasma flow energy E_V exceeds the plasma thermal energy E_T. We can not conclude the acceleration is electromagnetic or electrostatic only with the present experiment. In addition to that, it should be noted that, if the additional plasma production points propagate along the axis, we can not distinguish it from the plasma flow only by the time-of-flight estimation. Further investigation is needed to understand the ion acceleration mechanisms.

V. Conclusion

Applied and plasma-induced magnetic field distribution are measured in an electrodeless plasma thruster using a three-directional B-dot probe. Time- and space- resolved distributions of the azimuthal induced current are obtained using a Gaussian fitting analysis. Its distributions are in a good agreement with those of the azimuthal electric field, ensuring the inductive current drive. The ion dynamics are also investigated by the time-of-flight technique using the ion saturation current of a Langmuir probe. Without the external dc magnetic field, the ion flow velocity is estimated as comparable to the ion sound speed. In the external dc magnetic field, generation of supersonic ion flow is indicated.

References

[1] S. N. BATHGATE, M. M. M. BILEK, and D. R. MCKENZIE, "Electrodeless plasma thrusters for spacecraft: a review," *Plasma Sci. Technol.*, vol. 19, no. 8, p. 083001, Aug. 2017.

[2] C. R. Koppel and D. Estublier, "The smart-1 hall effect thruster around the moon: In flight experience," *29th Int. Electr. Propuls. Conf.*, pp. 1–9, 2005.
[3] H. Koizumi, K. Komurasaki, J. Aoyama, and K. Yamaguchi, "Development and Flight Operation of a Miniature Ion Propulsion System," *J. Propuls. Power*, vol. 34, no. 4, pp. 960–968, 2017.
[4] E. A. Bering *et al.*, "Performance studies of the VASIMR ® VX-200," *49th AIAA Aerosp. Sci. Meet. Exhib.*, no. January, pp. 4–7, 2011.
[5] J. Jarrige and D. Packan, "Geometry optimization and effect of gas propellant in an electron cyclotron resonance plasma thruster," pp. 1–12, 2017.
[6] K. Takahashi, A. Komuro, and A. Ando, "Operating a magnetic nozzle helicon thruster with strong magnetic field," *Phys. Plasmas*, vol. 23, no. 3, 2016.
[7] S. Shinohara *et al.*, "Development of featured high-density helicon sources and their application to electrodeless plasma thruster," *Plasma Phys. Control. Fusion*, vol. 61, no. 1, p. 014017, Jan. 2019.
[8] A. Fruchtman, K. Takahashi, C. Charles, and R. W. Boswell, "A magnetic nozzle calculation of the force on a plasma," *Phys. Plasmas*, vol. 19, no. 3, 2012.
[9] K. Takahashi, A. Chiba, A. Komuro, and A. Ando, "Experimental identification of an azimuthal current in a magnetic nozzle of a radiofrequency plasma thruster," *Plasma Sources Sci. Technol.*, vol. 25, no. 5, p. 055011, Aug. 2016.
[10] K. A. Polzin, "Comprehensive Review of Planar Pulsed Inductive Plasma Thruster Research and Technology," *J. Propuls. Power*, vol. 27, no. 3, pp. 513–531, 2011.
[11] E. Y. Choueiri and K. A. Polzin, "Faraday Acceleration with Radio-frequency Assisted Discharge (FARAD)," 2008.
[12] K. Yaginuma, H. Kurashige, H. Sekine, H. Koizumi, and K. Komurasaki, "Experimental Evaluation of Steady-State Electromagnetically Inductive Acceleration for Electrodeless Plasma Thruster and Fundamental Measurement of the Correlation between the Effective Current of Acceleration Coil and Thrust," *J. Japan Soc. Aeronaut. Sp. Sci.*, vol. 67, no. 1, pp. 25–34, 2019.
[13] K. Takahashi, A. Chiba, A. Komuro, and A. Ando, "Experimental identification of an azimuthal current in a magnetic nozzle of a radiofrequency plasma thruster," *Plasma Sources Sci. Technol.*, vol. 25, no. 5, 2016.
[14] H. Sekine, H. Koizumi and K. Komurasaki, "Inductive current drive and azimuthal electrical conductivity enhancement in an electrodeless radio-frequency plasma thruster," *Phys. Plasmas*, submitted.